Dispersion of Electric-Field-Induced Faraday Effect in Magnetoelectric Cr_{2}O_{3}

Junlei Wang and Christian Binek

Phys. Rev. Applied **5**, 031001 — Published 30 March 2016

DOI: 10.1103/PhysRevApplied.5.031001

Dispersion of electric field induced Faraday effect in magnetoelectric Cr_2O_3

Junlei Wang, Christian Binek

Department of Physics and Astronomy, University of Nebraska-Lincoln, Lincoln, NE 68588

Abstract

The frequency dependence of the electric field induced magneto-optical Faraday effect is investigated in the magnetoelectric antiferromagnet chromia. Two electrically induced Faraday signals superimpose in proportion to the linear magnetoelectric susceptibility, α, and the antiferromagnetic order parameter, η. The relative strength of these contributions is determined by the frequency of the probing light and can be tuned between extreme characteristics following the temperature dependence of α or η. The frequency dependence is analyzed in terms of electric dipole transitions of perturbed Cr^{3+} crystal-field states. The results allow measuring voltage-controlled selection, isothermal switching, and temperature dependence of η in a table-top setup. The voltage-specific Faraday rotation is independent of the sample thickness making the method scalable and versatile down to the limit of dielectric breakdown.

PACs: 78.20.Ls, 75.50.Ee, 75.85.+t.

Electric field induced Faraday rotation is a fascinating phenomenon in magnetoelectrics with antiferromagnetic (AFM) spin order. Little is known about the dispersion of this magneto-optical effect. Theory suggests that dispersion can be utilized to tune into a regime where the Faraday signal is proportional to the AFM order parameter, η. Measuring the orientation of η is a notoriously difficult problem in condensed matter physics. This is largely because perfect AFM spin order leads to vanishing net magnetization thus ruling out standard magnetometry as characterization technique. Experiments discriminating two degenerate AFM 180 degree domains have proven challenging. This holds particularly in thin film magnetism where AFM constituents allow for the potentially advantageous variation of AFM spintronics [1-3] or applications such as voltage-controlled ultra-low power spintronics [4-6].

Established methods which allow measurement of η include neutron diffraction, x-ray linear magnetic dichroism (XMLD), and optical second harmonic generation. Both, neutron diffraction and XMLD require large-scale research facilities. While neutron diffraction topography suffers from the need of long exposure times [7], XMLD has other shortcomings. It senses spin alignment via charge distribution [8,9]. The situation has been improved with the advent of nonlinear optical topography first applied for the magnetoelectric (ME) antiferromagnet Cr_2O_3 (chromia) [10]. In ME antiferromagnets time and spatial inversion symmetry are broken below the Néel temperature, T_N. Their combined application leaves the AFM spin structure invariant [11]. These symmetry requirements allow for electric-field (E) induced magnetization $\mu_0 \underline{M} = \underline{\underline{\alpha}}\, \underline{E}$, where α is the ME susceptibility. Fiebig et al. were able to generalize their method when relaxing the previously required symmetry constraints of ME antiferromagnets through extrinsic experimental refinements [12]. This makes second harmonic generation a powerful

method of topography. It lacks, however, the ability to determine the sign of η. In addition, all of the above methods are not suitable for investigations of thin film samples.

In this letter we investigate the DC electric field-induced Faraday effect (EFIF) and its dispersion. Specifically, the temperature (T) dependence of the Faraday rotation, Θ, of the ME antiferromagnet chromia is studied on variation of the frequency, ω, of the probing light. A fundamental insight gained from the analysis of $\Theta(T)$ for light frequencies $10000 < \omega < 12500\ \mathrm{cm}^{-1}$ is the ability to tune ω into a regime where $\theta \propto \eta$. With this finding we establish a compact method sensitive to measure sign and magnitude of η in the ME antiferromagnet chromia and potentially other ME antiferromagnets [13]. Our results demonstrate dispersion of the EFIF and enable voltage-controlled selection, isothermal switching, and measurement of the T-dependence of η. These capabilities have significance for the investigation of AFM spin structures and the development of applications aiming at voltage-control of memory and logical states via switching of AFM domain states. Recently, non-volatile ultra-low power memory and logical devices have been proposed. They employ the ME effect and the associated voltage-controlled AFM order parameter switching in thin film heterostructures for virtually dissipationless switching of state variables. ME devices encode information in remnant and thus non-volatile magnetization states providing additional functionality over CMOS counterparts. In ME devices, voltage-controlled non-linear switching of boundary magnetization, a generic property of ME antiferromagnets [14-16], is mapped onto voltage-controlled switching between remnant magnetization of an adjacent ferromagnetic (FM) thin film through quantum mechanical exchange at the AFM/FM interface. It gives rise to voltage-controlled exchange bias [15,17,18] enabling, e.g, ultra-low power ME magnetic random access memory, majority gates, and other ME variations of memory and logic device applications [4,5].

The Faraday effect is, next to the Kerr effect, among the commonly exploited methods to characterize magnetic materials. Faraday and Kerr effect are in the class of rare non-reciprocal optical phenomena [19,20]. Faraday rotation refers to the rotation of the polarization plane of linearly polarized light transmitted through a magnetized sample. ME antiferromagnets show an *E*-field induced Faraday effect [21]. In contrast to ordinary Faraday rotation, EFIF takes place in the absence of an applied magnetic field or sample inherent magnetization. Two distinct mechanisms constitute the total *E*-field induced rotation. These are the magnetization induced by the ME effect with a *T*-dependence following $\alpha(T)$ and an *E*-field induced pseudo-Stark effect which creates rotation with a *T*-dependence proportional to $\eta(T)$. The understanding of EFIF is best developed for the archetypical ME antiferromagnet Cr_2O_3 [11,21,22]. Despite the groundbreaking previous work, experimental investigations of dispersion of EFIF are still lacking, even in the archetypical Cr_2O_3. It is the prime objective of this work to fill in this gap. To bring our experiments in the context of the theoretical framework we briefly recapitulate the phenomenology and microscopic origin of the EFIF [21].

EFIF, like all Faraday rotation, originates from the difference, $\Delta n = n_+ - n_-$, in the refractive indices for positive (+) and negative (-) circularly polarized light. Δn can be traced back to the presence of complex off-diagonal elements in the dielectric tensor, ϵ_{ij}. The elements, $\epsilon_{xy} = -\epsilon_{yx}$ can be expressed as $\epsilon_{xy} = ig_z$, where g_z is the *z*-component of the gyrotropic vector. In uniaxial ferromagnets with magnetization *M* along the *z*-axis, Faraday rotation is proportional to *M* in accordance with $g_z \propto M$ and $g_z \ll \epsilon_{xx}$. In analogy to Faraday rotation in uniaxial ferromagnets one expects for a uniaxial antiferromagnet with sublattice magnetizations $M_{A,B}$ that $g_z = 2(p_A M_A + p_B M_B)$ where z corresponds to the *c*-axis in chromia. In $E_z = 0$ the coefficients $p_{A,B}$ are degenerate according to $p_A = p_B = p$. Because $M_B = -M_A$ in zero fields

this yields vanishing Faraday rotation in antiferromagnets. Note that although η of chromia is composed from 4 sublattices [21] it is sufficient for our purpose to distinguish sites with up and down spins [21]. An applied electric field, E_z, induces $\theta \neq 0$ in H=0 for ME antiferromagnets such as chromia. In chromia, the E-field displaces the Cr^{3+} ions along the 3-fold c-axis moving them into different crystal-field environments. The dissimilar crystal-field lifts the degeneracy of A (up spins) and B sites (down spins) resulting in $p_{A,B} = p \pm qE_z$ [21]. When eliminating $M_{A,B}$ in $g_z = 2(p_A M_A + p_B M_B)$ via $M_z = M_A + M_B = \alpha E_z$ and $\eta = M_A - M_B$, the z-component of the gyrotropic vector reads $g_z = 2(p\alpha E_z + q\eta E_z)$. It provides the phenomenological functional form

$$\Theta = K\mathrm{d}(p\alpha E_z + q\eta E_z), \tag{1}$$

of EFIF, where K is a proportionality constant.

Microscopically, Faraday effects are based on electric dipole transitions [23]. From crystal field theory of chromium trihalides and similarly for chromia it is known that an appreciable Faraday effect originates from the average dipole moment of *d-d* transitions [21,24]. In chromia these are the transitions between the ground state, ${}^4A_2$, and excited states of ${}^4T_2$-type of the Cr^{3+} ions. The ${}^4A_2$ and ${}^4T_2$ states split in the trigonal crystal field perturbed by spin-orbit interaction and exchange interaction. In addition they experience a Stark-like shift in response to an applied E-field [21]. Based on this crystal-field theory, the ω-dependence of p and q has been worked out and reads

$$p(\omega) = \frac{2\pi\omega}{n\hbar c} p_\alpha^2 \left\{ \frac{1}{\omega_{C(\alpha)}^2 - \omega^2} - \sum_{i=1}^{3} \frac{a_{A_i(\alpha)}}{\omega_{A_i(\alpha)}^2 - \omega^2} \right\} \tag{2}$$

$$q(\omega) = \frac{2\pi\omega}{n\hbar c} p_\alpha^2 \left\{ \frac{|A_1^0|(\chi_0+\chi_C)}{\left(\omega_{C(\alpha)}^2-\omega^2\right)^2} - \sum_{i=1}^{3} \frac{a_{A_i(\alpha)}^2 |A_1^0|(\chi_0+\chi_{A_i})}{\left(\omega_{A_i(\alpha)}^2-\omega^2\right)^2} \right\}, \quad (3)$$

where $\omega_{C(\alpha)}$ and $\omega_{A_i(\alpha)}$ are transition frequencies from the ground state to the states $C(\alpha) = C(m = \pm 5/2)$ and $A_{1,2,3}(\alpha) = A_{1,2,3}(m = \pm 1/2)$, respectively. Here m is the quantum number of the z-component of the angular momentum. The notation in Eqs. (2) and (3) has been adopted from [21]. Specifically, $|A_1^0|(\chi_0 + \chi_{A_i})$ quantifies the pseudo-Stark splitting, i.e. a mere positive (negative) E-field induced linear shift between the energy levels, of the levels of Cr^{3+} ions on A (B) sides excited via circularly polarized light. Next we provide an approximation for p/q using assumptions previously applied in Ref. [21]. Considering that the splitting of the ${}^4T_2$ level in the trigonal field is much greater than the spin-orbit splitting it follows for the square of the transition matrix elements $\alpha_{A_2}^2 \approx \alpha_{A_3}^2 \approx 0$. From the previous assumption that mixing of wave functions is virtually identical for the most relevant excited states C and A follows $\chi_C \approx \chi_A$. With these approximations, p/q simplifies into

$$\frac{p(\omega)}{q(\omega)} = \frac{1}{|A_1^0|(\chi_0 + \chi_C)} \frac{(\omega_C^2 - \omega^2)(\omega_A^2 - \omega^2)}{\omega_A^2 - \omega^2 + a_{A_1}(\omega_C^2 - \omega^2)} \quad (4)$$

We experimentally explore the ω-dependence of Eq. (4) via spectroscopy of EFIF by utilizing laser light sources with wavelengths λ=804, 830, 852, 905, 940 and 980 nm. The setup is shown in **Fig. 1**. We employ photo-elastic modulation and phase-sensitive lock-in technique to measure the EFIF effect. The polarization modulated light is transmitted along the c-axis of the chromia sample which resides in a custom made UHV chamber with optical windows.

Prior to each measurement, the (0001) oriented chromia single crystal, which has a semitransparent Platinum electrode deposited on each (0001) surface, is prepared in an AFM single domain state via ME annealing [25]. Electric (E=±3 kV/mm) and magnetic fields

($\mu_0 H$ =±150 mT) are simultaneously applied along the [0001]-direction (*c*-axis) on cooling from $T = 340$ K $> T_N = 308$K to $T = 280$ K $< T_N$. Cooling takes place at speed $|dT/dt|$<5 K/min to avoid quenching into a multi-domain state. ME annealing selects the registration of η through the sign of the sufficiently large *EH*-product. At *T*=280K when long-range AFM order has been established, fields are switched off and cooling continues in *E*=*H*=0 to $T \approx 100$ K. Once the system equilibrates, EFIF is measured on heating.

Fig. 2 shows a typical result of the *T*-dependent EFIF measured with laser light of $\lambda = 980$ nm. At each temperature, Θ versus applied voltage, *V,* is measured. DC electric fields $E = V/d$ are applied along the *c*-axis through quasi-static variation of applied voltages within $50V < V < 1500V$ where $d = 0.5$ mm is the thickness of the chromia single crystal. Note that our DC technique, although experimentally more challenging than AC techniques, has particular advantages. In a DC measurement Θ vs *V* rather than dΘ/*dV* vs *V* is measured. Even though the implications of this fundamental difference are not further investigated in this letter it is worth to mention that Θ vs *V* is free from dynamic anomalies and sensitive to *V*-independent Θ-contributions. An important example is the Θ-contribution originating from boundary magnetization which accompanies the bulk AFM order parameter in ME antiferromagnets [16,26]. The DC method has the capability to correlate boundary magnetization and η. A representative data set of a quasi-static Θ vs *V* measurement at *T*= 250 K is shown in the inset of Fig2. The Θ vs *V* isotherm determines the individual data point circled in the main panel of Fig. 2. In accordance with Eq. (1), Θ depends linearly on *E* and thus linearly on *V*. Hence, a linear best fit of Θ vs *V* provides the voltage-specific (Sp.) EFIF $d\Theta/dV$ according to

$$\frac{\mathrm{d}\Theta}{\mathrm{d}V} = \frac{\mathrm{d}\Theta}{\mathrm{d}E}\frac{\mathrm{d}E}{\mathrm{d}V} = K(p\alpha + q\eta) \qquad (5)$$

Note that $\mathrm{d}\Theta/\mathrm{dV}$ is a thickness independent specific Faraday rotation. Invariance of $\mathrm{d}\Theta/\mathrm{dV}$ with respect to thickness scaling makes this method suitable for thin film investigations provided the dielectric properties of the films allow maintaining voltages similar to those applied in the bulk single crystal. While high voltages at the nanoscale are out of reach, electric fields in excess of 250kV/mm have been applied across chromia (0001) films corresponding to voltages >100V for films of <500nm thickness [17,18]. Squares and circles in Fig. 2 show $\mathrm{d}\Theta/\mathrm{d}V$ vs. T for the two distinct 180 degree single domain states selected by respective ME annealing in $EH < 0$ (squares) and $EH > 0$ (circles). The two data sets show virtually perfect mirror symmetry relative to the T-axis reflecting the fact that both α and η flip sign when switching from one AFM single domain state to the degenerate other. The prominent cut-off behavior in $\mathrm{d}\Theta/\mathrm{dV}$ vs T given by $\mathrm{d}\Theta/\mathrm{dV} = 0$ for $T > T_N$ indicates that $\alpha = \eta = 0$ above T_N. This is in accordance with the necessary condition that EFIF requires broken time inversion symmetry as a result of spontaneous symmetry breaking accompanying the second order AFM to paramagnetic phase transition.

The solid lines in **Fig. 2** are least squares fits of Eq.(5) to the $d\Theta/\mathrm{dV}$ vs T data. In order to convert Eq. (5) into an explicit T-dependent function we employ $\eta(T) = \eta_0(T_N - T)^{\beta}$ with $\beta = 0.355$ (Fig. 2 dot-dashed line) [27]. To obtain a parameter free function for $\alpha(T)$, we employ the phenomenological product representation $\alpha = \alpha_0\eta(T)\chi(T)$ of the parallel ME susceptibility [28]. Here, α_0 is a constant and $\chi(T)$ is the parallel magnetic susceptibility. We use an analytic approximation given by the Firgau formula which is exact for Ising models on a Bethe lattice. The Firgau approximation is of sufficient accuracy because details of the criticality leave the global T-dependence of the EFIF virtually unaffected [29,30]. The analytic expression $\alpha(T) = \alpha_0\eta(T)\chi(T)$ is fitted to experimental data of the ME susceptibility measured by Borisov

et al. with the help of a modified AC SQUID method of high accuracy and precision [31]. The result of this fit is shown in Fig. 2 (dashed line). It becomes a parameter-free input for the least square fit of Eq.(5) to our Sp. EFIF data. The least squares fit of Eq.(5) involves the free parameters $P_1 = K \cdot p$ and $P_2 = K \cdot q$. The results show perfect agreement with our data within their noise level. The fit allows decomposition of $\mathrm{d}\Theta/\mathrm{d}V$ vs. T for each wavelength into the ME and the order parameter component, respectively. The components provide the ratio p/q.

Fig. 3(a)-(f) show the $\mathrm{d}\Theta/\mathrm{d}V$ vs. T data and corresponding best fits for λ=804, 830, 852, 905, 940 and 980 nm, respectively. The resulting ratios, p/q, of the least squares fits are summarized in the Table and plotted in **Fig. 4**a (circles) as function of light frequency (and wavelength). We fit the data points using Eq. (4) to determine $\omega_C = 11584\ \mathrm{cm}^{-1}$, $\omega_A = 11213\ \mathrm{cm}^{-1}$, and the value of the matrix element $a_{A_1} = -0.904$. The results of the best fits agree with the assumptions $\omega_C \approx \omega_A$ and $|a_{A_1}| \sim 1$. The latter is in accordance with $\alpha_{A_2}^2 \approx \alpha_{A_3}^2 \approx 0$ due to the constraint $\alpha_{A_1}^2 + \alpha_{A_2}^2 + \alpha_{A_3}^2 = 1$.

The frequency dependence of p/q shown in Fig. 4a implies $p/q \to 0$ for light frequencies near $\omega = 11050\ \mathrm{cm}^{-1}$ (λ= 905 nm). Here the EFIF is directly proportional to the η as reflected by the order parameter characteristics of $\mathrm{d}\Theta/\mathrm{d}V$ vs T in Fig. 3 (d). It is interesting to note that $\mathrm{d}\Theta/\mathrm{d}V$ maximizes at λ= 905 nm (see Fig.3) together with the minimizing of p/q. This correlation is consistent with the crystal field theory predicting large Faraday rotation near the same *d-d* transitions which determine the dispersion of the EFIF. It is tempting to assume that the transition frequencies entering Eq.(4) can be inferred from the optical absorption spectrum measured in [32] in E=0. However, it is important to keep in mind that the pseudo Stark shift has a drastic but hitherto ill-quantified effect on ω_C and ω_A as reported in [21,33]. It prevents a quantitative comparison between our fitting results and the spectroscopy in E=0. The possibility

to tune into the regime where the *T*-dependence of $\mathrm{d}\Theta/\mathrm{d}V$ is solely determined by $\eta(T)$ makes electric field induced Faraday rotation an ideal tool to study the AFM order parameter. Additionally, EFIF in general is a table-top technique to distinguish the two 180 degree AFM single domain states, not just as a domain contrast but in terms of the sign of η of an individual AFM single domain. Of particular interest is monitoring isothermal switching of η shown in Fig. 4b. An AFM single domain state with $\eta > 0$ has been selected via ME annealing from *T*=340 to 305K in *E*= 1.6kV/mm and $\mu_0 H = -110$ mT. After annealing (see Fig. 4c for protocol), the fields have been removed and Θ vs. *V* is measured isothermally (circles Fig. 4b). The positive slope of Θ vs. *V* indicates that annealing selected an AFM single domain state with $\eta > 0$. Next, the sample has been exposed at *T*=305K to an axial field product *EH* > 0 with in *E*= 1.6kV/mm and $\mu_0 H = +110$ mT resulting in a Θ vs. *V* isotherm of negative slope (squares Fig. 4b). The change in slope is indicative of isothermal switching into a single domain state with $\eta < 0$.

Gyrotropic birefringence has been proposed to measure η in chromia. However, the difference in rotation of the indicatrix associated with the AFM order and the resulting contribution to the birefringence are small and plagued by parasitic background signals hampering any attempt to quantitatively investigate $\eta(T)$ [22]. In contrast, the simplicity and scalability of EFIF opens the unique possibility to employ the method for technologically relevant AFM thin films.

In conclusion, we investigated dispersion of the electric field induced Faraday effect in the magnetoelectric antiferromagnet Cr_2O_3 and experimentally verified the frequency dependence predicted in the framework of a crystal-field theory. Our spectroscopic data confirm that the Faraday signal is composed of two electric field induced components which exhibit the temperature dependence of the magnetoelectric susceptibility and the antiferromagnetic order

parameter of Cr_2O_3. We demonstrate that the two contributions dependent dissimilarly on the frequency of the probing light and analyze our data in the framework of electric dipole transitions between crystal-field states of the magnetic Cr^{3+} ion. We demonstrate that selection of the laser light frequency allows tuning into a regime where the specific Faraday rotation is directly proportional to the antiferromagnetic order parameter. This enables a convenient, table-top approach to measure the antiferromagnetic order parameter and its switching, e.g., by pure electrical means. Implications range from domain topography, to reference free measurement of the orientation of the antiferromagnetic order parameter, to measurements of its isothermal switching. Voltage-controlled switching of the antiferromagnetic spin structure enables spintronic devices such as ultra-low power magnetic random access memories, majority gates, and logical devices. Understanding of the voltage-induced reversal of the order parameter in magnetoelectric antiferromagnets is of key importance to advance this promising branch of voltage-controlled spintronics.

Acknowledgements

This project is supported by the Nanoelectronics Research Initiative (NRI), a Semiconductor Research Corporation program (SRC), via the CNFD through tasks SRC 2398.001 and 2587.001, by C-SPIN, one of six centers of STARnet, a SRC program, sponsored by MARCO and DARPA, and by NSF through Nebraska MRSEC DMR-1420645. The research was performed in part in the Nebraska Nanoscale Facility, Nebraska Center for Materials and Nanoscience, which is supported by the National Science Foundation under Award NNCI: 1542182, and the Nebraska Research Initiative.

Figure Captions:

Fig. 1: Optical setup for EFIF effect. L: laser; P: polarizer; PEM: photoelastic modulator; M: electro-magnet; S: sample inside UHV chamber; A: analyzer with automated rotational stage; PD: photodetector; DMM: digital Multimeter; LiA: lock-in amplifier.

Fig. 2: Temperature dependence of the Sp. EFIF of Cr_2O_3 measured with light of 980 nm wavelength for the two degenerate AFM single domain states with positive (square) and negative (circles) η selected via field cooling in $EH<0$ and $EH>0$. Solid lines (color online) show best fits of Eq. (5). Dashed line shows contribution proportional to $\alpha(T)$. Dot-dashed line shows component proportional to $\eta(T)$. The inset displays EFIF as function of applied voltage measured at $T = 250$ K.

Fig. 3: Temperature dependence of Sp. EFIF probed with light at (a) 804 nm, (b) 830 nm, (c) 852 nm, (d) 905 nm, (e) 940 nm and (f) 980 nm, respectively. Circles represent data points obtained from isothermal EFIF measurements, respectively. Solid lines show best fits of Eq. (5). Respective ratios of the two free fitting parameters are summarized in the Table.

Fig. 4: (a) Ratio of the fitting parameters p/q as a function of frequency (wavelength) of the probing light. Solid line is the best fit of Eq.(4). (b) Isothermal Θ vs. V data measured at T=305K following the field-protocol shown in (c) which results in switching of η between $\eta > 0$ (circles) and $\eta < 0$ (squares).

Wavelength (nm)	804	830	852	905	940	980
Frequency (cm^{-1})	12437.8	12048.2	11737.1	11049.7	10638.3	10204.1
p/q	1.429	0.633	0.165	-0.001	1.188	2.974

Table. Summary of fitting result.

References

[1] Z. Wei, A. Sharma, A. S. Nunez, P. M. Haney, R. A. Duine, J. Bass, A. H. MacDonald, and M. Tsoi, Changing Exchange Bias in Spin Valves with an Electric Current, Phys Rev Lett **98**, 116603 (2007).

[2] X. Marti, I. Fina, and T. Jungwirth, Prospect for Antiferromagnetic Spintronics, Magnetics, IEEE Transactions on **51**, 1 (2015).

[3] E. V. Gomonay and V. M. Loktev, Spintronics of antiferromagnetic systems (Review Article), Low Temperature Physics **40**, 17 (2014).

[4] P. A. Dowben, C. Binek, and D. E. Nikonov, in *Nanoscale Silicon Devices*, edited by S. Oda, and D. K. Ferry (CRC Press, Boca Raton, FL, 2015).

[5] C. Binek and B. Doudin, Magnetoelectronics with magnetoelectrics, J Phys-Condens Mat **17**, L39 (2005).

[6] W. Kleemann and C. Binek, in *Magnetic Nanostructures*, edited by H. Zabel, and M. Farle (Springer Berlin Heidelberg, 2013), pp. 163.

[7] J. Baruchel, M. Schlenker, and W. L. Roth, Observation of Antiferromagnetic Domains in Nickel-Oxide by Neutron-Diffraction Topography, J Appl Phys **48**, 5 (1977).

[8] P. Kuiper, B. G. Searle, P. Rudolf, L. H. Tjeng, and C. T. Chen, X-ray magnetic dichroism of antiferromagnet Fe_2O_3: The orientation of magnetic moments observed by Fe 2p x-ray absorption spectroscopy, Phys Rev Lett **70**, 1549 (1993).

[9] M. M. Schwickert, G. Y. Guo, M. A. Tomaz, W. L. O'Brien, and G. R. Harp, X-ray magnetic linear dichroism in absorption at the L edge of metallic Co, Fe, Cr, and V, Phys Rev B **58**, R4289 (1998).

[10] M. Fiebig, D. Fröhlich, G. Sluyterman v. L, and R. V. Pisarev, Domain topography of antiferromagnetic Cr_2O_3 by second-harmonic generation, Appl Phys Lett **66**, 2906 (1995).

[11] T. H. O'Dell and E. A. D. White, Electric field induced faraday rotation in chromic oxide, Philos. Mag. **22**, 649 (1970).

[12] M. Fiebig, D. Fröhlich, S. Leute, and R. V. Pisarev, Topography of antiferromagnetic domains using second harmonic generation with an external reference, Applied Physics B **66**, 265 (1998).

[13] J. Wang, J. A. Santana, N. Wu, C. Karunakaran, J. Wang, P. A. Dowben, and C. Binek, Magnetoelectric Fe_2TeO_6 thin films, Journal of physics. Condensed matter : an Institute of Physics journal **26**, 055012 (2014).

[14] N. Wu, X. He, A. L. Wysocki, U. Lanke, T. Komesu, K. D. Belashchenko, C. Binek, and P. A. Dowben, Imaging and Control of Surface Magnetization Domains in a Magnetoelectric Antiferromagnet, Phys Rev Lett **106** (2011).

[15] X. He, Y. Wang, N. Wu, A. N. Caruso, E. Vescovo, K. D. Belashchenko, P. A. Dowben, and C. Binek, Robust isothermal electric control of exchange bias at room temperature, Nat Mater **9**, 579 (2010).

[16] K. D. Belashchenko, Equilibrium Magnetization at the Boundary of a Magnetoelectric Antiferromagnet, Phys Rev Lett **105**, 147204 (2010).

[17] K. Toyoki, Y. Shiratsuchi, A. Kobane, C. Mitsumata, Y. Kotani, T. Nakamura, and R. Nakatani, Magnetoelectric switching of perpendicular exchange bias in Pt/Co/α-Cr_2O_3/Pt stacked films, Appl Phys Lett **106**, 162404 (2015).

[18] T. Ashida, M. Oida, N. Shimomura, T. Nozaki, T. Shibata, and M. Sahashi, Isothermal electric switching of magnetization in Cr_2O_3/Co thin film system, Appl Phys Lett **106**, 132407 (2015).

[19] V. N. Muthukumar, R. Valenti, and C. Gros, Theory of nonreciprocal optical effects in antiferromagnets: The case of Cr_2O_3, Phys Rev B **54**, 433 (1996).

[20] V. V. Eremenko, Y. G. Litvinenko, N. K. Kharchenko, and V. M. Naumenko, (Springer New York, New York, NY, 1992), p. 276.

[21] B. B. Krichevtsov, V. V. Pavlov, and R. V. Pisarev, Nonreciprocal optical effects in antiferromagnetic Cr_2O_3 subjected to electric and magnetic fields, Sov. Phys. JETP **67**, 378 (1988).

[22] R. V. Pisarev, Crystal optics of magnetoelectrics, Ferroelectrics **162**, 191 (1994).

[23] Y. R. Shen, Faraday Rotation of Rare-Earth Ions. I. Theory, Phys. Rev. **133**, A511 (1964).

[24] J. F. Dillon Jr, H. Kamimura, and J. P. Remeika, Magneto-optical properties of ferromagnetic chromium trihalides, Journal of Physics and Chemistry of Solids **27**, 1531 (1966).

[25] T. J. Martin and J. C. Anderson, Magneto-Electric Annealing Effects of Cr_2O_3, Phys. Lett. **11**, 109 (1964).

[26] X. He, Y. Wang, N. Wu, A. N. Caruso, E. Vescovo, K. D. Belashchenko, P. A. Dowben, and C. Binek, Robust isothermal electric control of exchange bias at room temperature, Nat Mater **9**, 579 (2010).

[27] R. V. Pisarev, B. B. Krichevtsov, and V. V. Pavlov, Optical Study of the Antiferromagnetic-Paramagnetic Phase-Transition in Chromium-Oxide Cr_2O_3, Phase Transit **37**, 63 (1991).

[28] Note that the representation $\alpha=\alpha_0\,\eta(T)\chi(T)$ is an approximation which formally allows to express the specific EFIF as $d\Theta/dV=K(p\chi(T)+q)\eta$. We prefer Eq.(5) over the factorized representation because the former expresses the distinctly different microscopic origin of the terms $p\alpha$ and $q\eta$.

[29] M. E. Fisher, Perpendicular Susceptibility of the Ising Model, Journal of Mathematical Physics **4**, 124 (1963).

[30] U. Firgau, Zur Theorie des Ferromagnetismus und Antiferromagnetismus, Annalen der Physik **432**, 295 (1941).

[31] P. Borisov, A. Hochstrat, V. V. Shvartsman, and W. Kleemann, Superconducting quantum interference device setup for magnetoelectric measurements, Rev Sci Instrum **78**, 106105 (2007).

[32] D. S. McClure, Comparison of the Crystal Fields and Optical Spectra of Cr_2O_3 and Ruby, The Journal of Chemical Physics **38**, 2289 (1963).

[33] W. Kaiser, S. Sugano, and D. L. Wood, Splitting of the Emission Lines of Ruby by an External Electric Field, Phys Rev Lett **6**, 605 (1961).

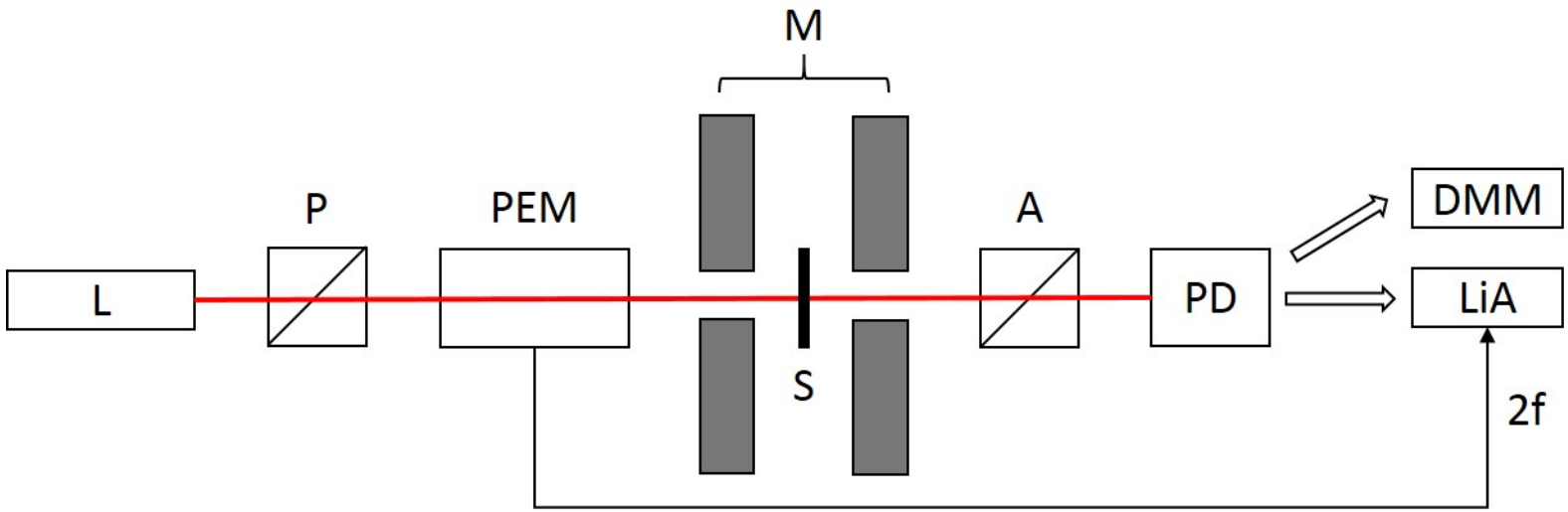

Figure 1

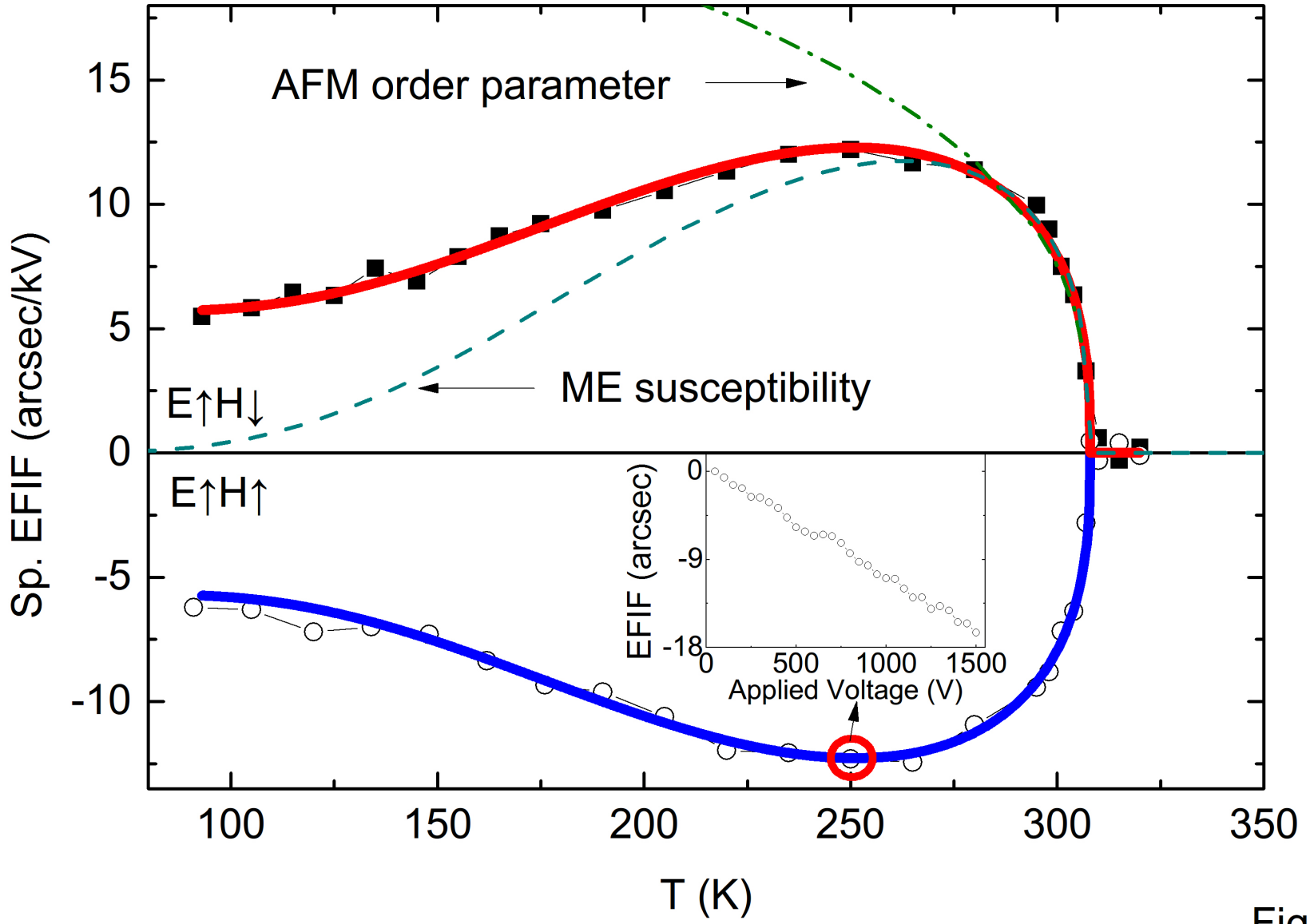
AFM order parameter
ME susceptibility
E↑H↓
E↑H↑
Sp. EFIF (arcsec/kV)
T (K)
EFIF (arcsec)
Applied Voltage (V)
15
10
5
0
-5
-10
100
150
200
250
300
350
0
-9
-18
500
1000
1500

Figure 2

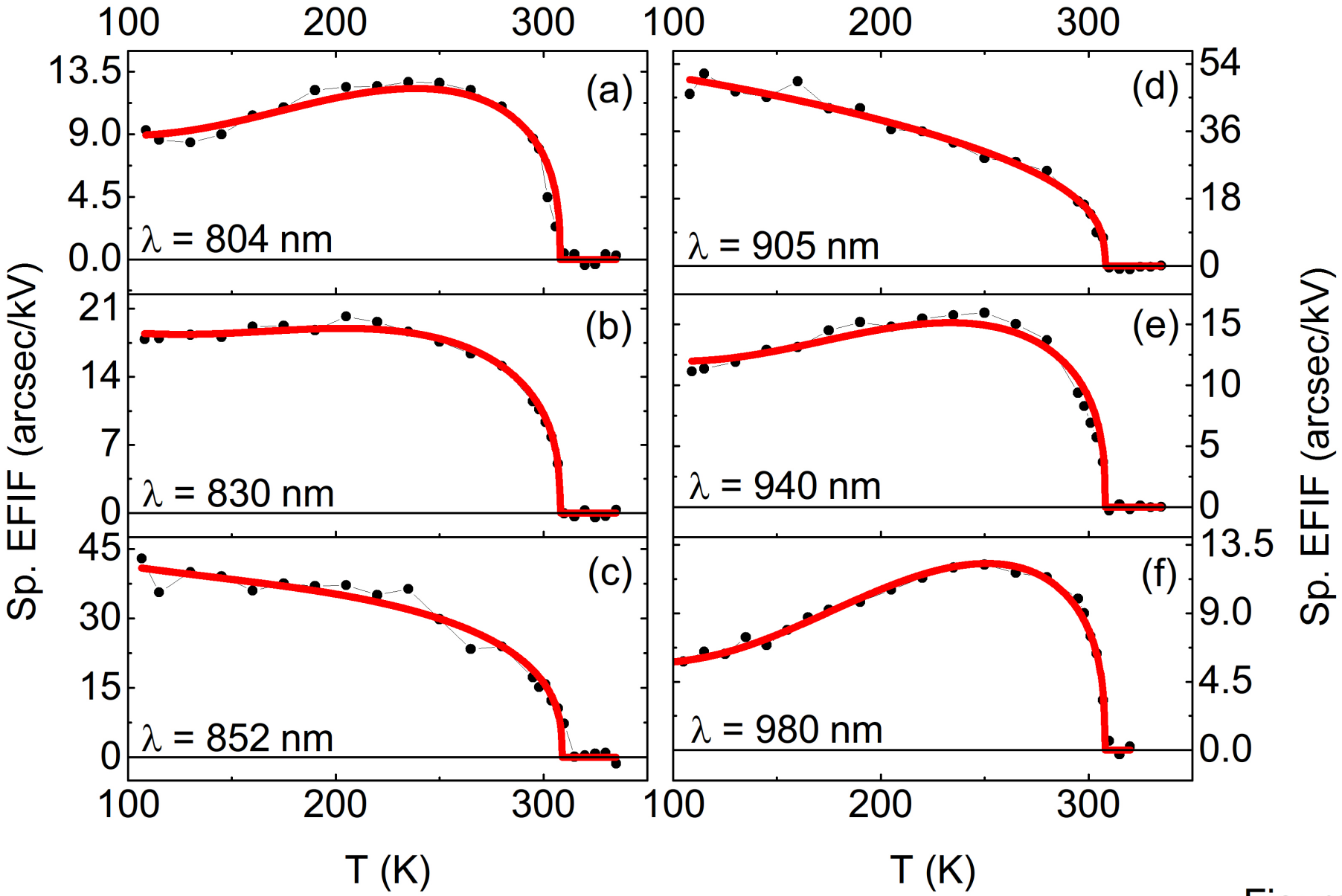
100
200
300
13.5
9.0
4.5
0.0
(a)
λ = 804 nm
21
14
7
0
(b)
λ = 830 nm
45
30
15
0
(c)
λ = 852 nm
54
36
18
0
(d)
λ = 905 nm
15
10
5
0
(e)
λ = 940 nm
13.5
9.0
4.5
0.0
(f)
λ = 980 nm
Sp. EFIF (arcsec/kV)
T (K)

Figure 3

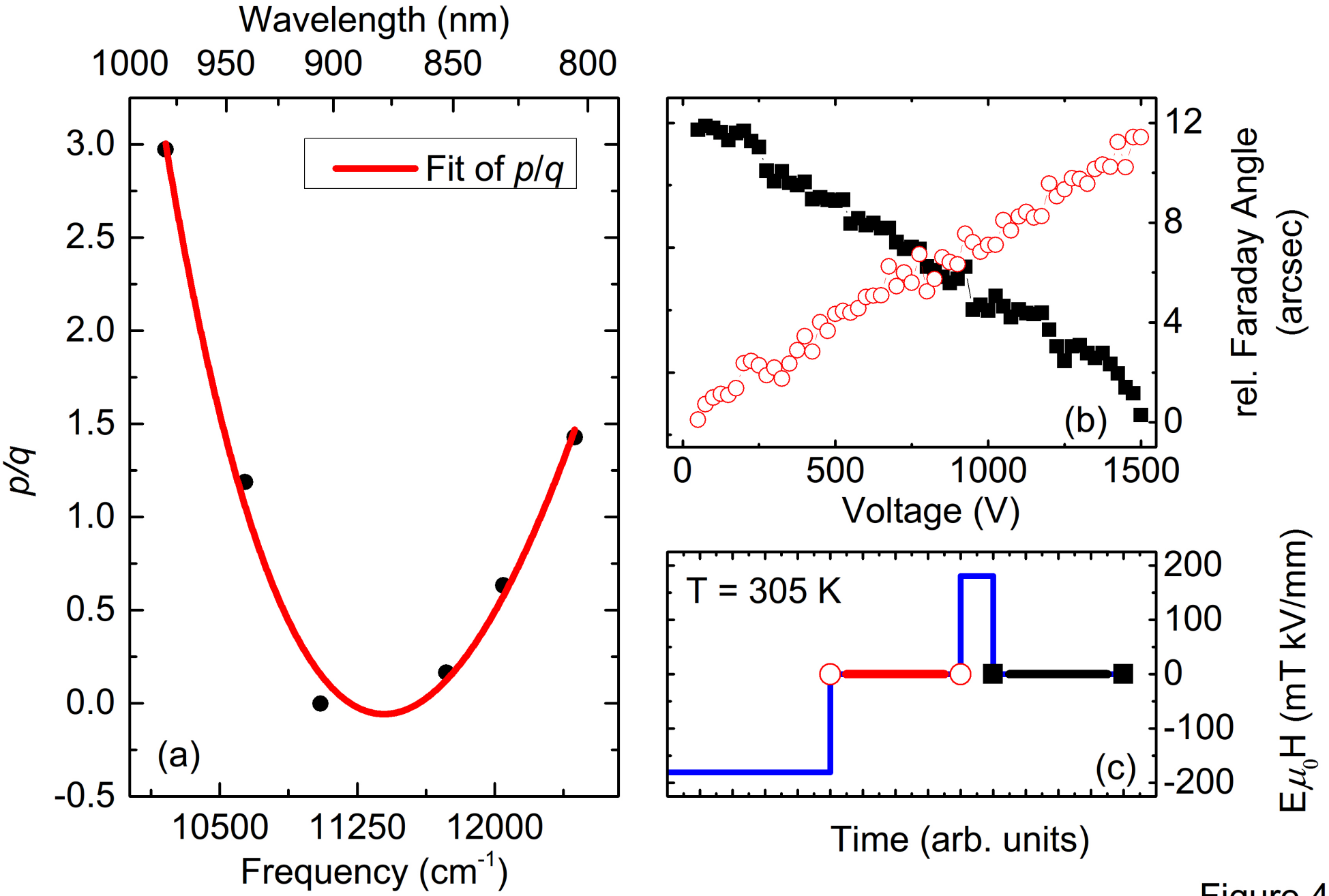
Wavelength (nm)
1000
950
900
850
800
Fit of p/q
p/q
3.0
2.5
2.0
1.5
1.0
0.5
0.0
-0.5
(a)
10500
11250
12000
Frequency (cm-1)
12
8
4
0
(b)
0
500
1000
1500
Voltage (V)
rel. Faraday Angle (arcsec)
T = 305 K
200
100
0
-100
-200
(c)
Time (arb. units)
Eμ0H (mT kV/mm)

Figure 4